

Experimental Observation of Nonlinear Synchronization due to a Single Wave

F. Doveil,* D.F. Escande,† and A. Macor‡

Physique des interactions ioniques et moléculaires, Unité 6633 CNRS-Université de Provence, Equipe turbulence plasma, case 321, Centre de Saint-Jérôme, F-13397 Marseille Cedex 20, France

(Received 4 November 2004; published 4 March 2005)

A test electron beam is propagated in a specially designed traveling wave tube. It interacts with a nonresonant wave, and its energy distribution is recorded at the tube output. We report the direct experimental observation of the spatially periodic electron velocity bunching, and of a nonlinear effect on the electron velocity modulation: the synchronization of the particles with the wave responsible for Landau damping in plasma physics. The results are explained by second order perturbation theory in the wave amplitude.

DOI: 10.1103/PhysRevLett.94.085003

PACS numbers: 52.40.Mj, 52.20.Dq, 52.35.Fp, 52.35.Mw

Wave-particle interaction plays an important role in accelerator physics and most plasma instabilities; it is central to the understanding of collective phenomena such as Landau damping [1]. While there were direct observations of trapping, i.e., resonant, effects during wave-particle interaction [2], in this Letter we report the first experimental evidence of the nonresonant, nonlinear electron velocity modulation by a single wave. This effect is important because, as recalled below, it is at the root of Landau damping in plasma physics [3–5].

We consider the interaction of essentially monokinetic electrons with one wave in a traveling wave tube (TWT). For a very weak electron beam intensity, the beam instability growth rate is negligible and electrons can be considered as test particles interacting with a constant amplitude wave. No self-consistent effect, usually responsible for wave amplification in a TWT, is taking place. Classical mechanics tells us that the motion of a charged particle in the frame moving at the wave phase velocity is the same as for the integrable nonlinear pendulum. The libration of the pendulum corresponds to the bouncing motion of the particle inside the wave potential trough. This well-known phenomenon is responsible for saturation of the most unstable wave in the self-consistent case [6], first observed in pioneering works on beam-plasma instability [7,8]. In this Letter, the mean beam velocity is very different from the wave phase velocity so that each beam electron is nonresonant, i.e., is far from being trapped. As expected, we observe a velocity modulation of the beam around its mean velocity v_b . This modulation is not symmetric around v_b . This nonlinear deviation is explained by second order perturbation theory in the wave amplitude.

The experiment is performed in a long TWT. It consists of three main elements: an electron gun, a slow wave structure (SWS) formed by a helix with axially movable antennas, and an electron velocity analyzer (Fig. 1). The central part of the electron gun consists of the grid-cathode subassembly of a ceramic microwave triode and the anode is replaced by a copper plate with an on-axis hole whose aperture defines the beam diameter equal to 3 mm. The

electron beam is confined by an axial magnetic field with typical amplitude 0.05 T strong enough for the beam radius to be set by the anode aperture as it propagates along the SWS axis. Beam current, $I_b < 1 \mu\text{A}$, and maximal cathode voltage, $|V_c| < 200 \text{ V}$, are set independently.

Waves are launched with a movable antenna. With the above parameters, the SWS is long enough to allow nonlinear processes to develop, as is shown later. It consists of a wire helix, rigidly held together by three threaded alumina rods and enclosed by a glass vacuum tube. The pressure at the ion pumps on both ends of the device is 2×10^{-9} Torr. The 4 m long helix is made of a 0.3 mm diameter Be-Cu wire; its radius is 11.3 mm and its pitch is 0.88 mm. Resistive rf terminations at each end of the helix reduce reflections. The maximal voltage standing wave ratio is 1.2 due to residual end reflections and helix irregularities. The glass vacuum jacket is enclosed by an axially slotted 57.5 mm radius cylinder that defines the rf ground. Inside this cylinder, but outside the vacuum jacket, are four axially movable antennas which are capacitively coupled to the helix and can excite or detect helix modes in the frequency range from 5 to 95 MHz. Only the helix

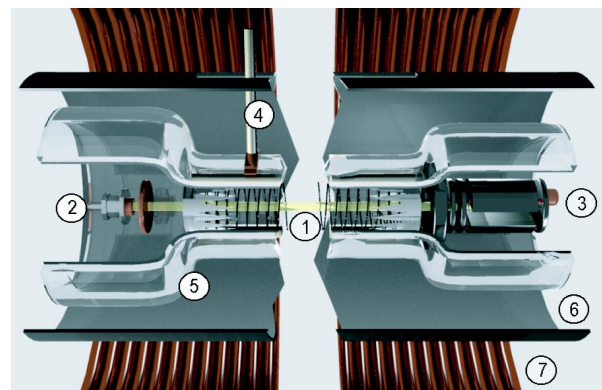


FIG. 1 (color online). Traveling wave tube rendering: (1) helix, (2) electron gun, (3) trochoidal analyzer, (4) antenna, (5) glass vacuum tube, (6) slotted rf ground cylinder, and (7) magnetic coil.

modes are launched, since empty waveguide modes can propagate only above 2 GHz. These modes have electric field components along the helix axis [6]. Launched electromagnetic waves travel along the helix at the speed of light; their phase velocities, v_ϕ , along the axis of the helix are smaller by approximately the tangent of the pitch angle, giving $2.8 \times 10^6 \text{ m/s} < v_\phi < 5.3 \times 10^6 \text{ m/s}$, since the electromagnetic signal covers a full helix circumference to perform one pitch length along the axis. Waves on the beamless helix are slightly damped, with $|k_{0i}|/|k_{0r}| \approx 0.005$, where $k_0 = k_{0r} + ik_{0i}$ is the beamless complex wave number. The dispersion relation closely resembles that of a finite radius, finite temperature plasma, with a nondispersive part close to origin followed by a second part with decreasing phase velocity [6], but, unlike plasma, the helix introduces no appreciable noise.

Finally, the cumulative changes of the electron beam distribution are measured with a trochoidal velocity analyzer [9], located at the end of the interaction region. It works on the principle that electrons undergo an $E \times B$ drift when passing through a region in which an electric field E is perpendicular to a magnetic field B . A small fraction (0.5%) of the electrons pass through a hole in the center of the front collector and are slowed down by three retarding electrodes. Then the electrons having the correct drift energy are collected after passing through an off-axis hole at the back of the analyzer. The time-averaged collected current directly gives the beam energy distribution function. Retarding potential and measured current are computer assisted, allowing an easy acquisition and treatment with energy resolution lower than 0.5 eV.

For a single wave with constant amplitude and frequency $f = 30 \text{ MHz}$ launched by a fixed probe at $L = 50 \text{ cm}$ from the output of the device, the velocity distribution function (VDF) of the test electron beam is measured at the device output. This procedure averages out the linear sloshing of particles due to the wave. Figure 2(a) plots, for different wave amplitudes, the VDF detected by the trochoidal analyzer. It is the result of superposing measurements obtained for different wave amplitudes of the single wave varying from 0 mV to 45 mV by steps of 3 mV. For

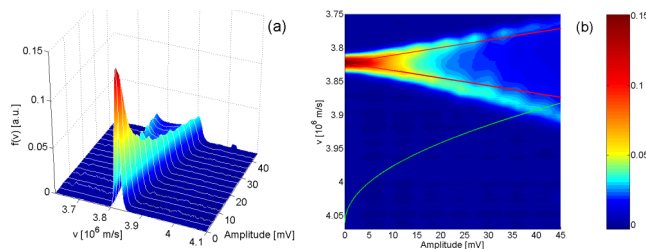


FIG. 2 (color online). Measured velocity distribution function in a single wave at $v_\phi = 4.06 \times 10^6 \text{ m/s}$ with increasing amplitude: (a) 3D plot, (b) 2D plot with first order estimates of modulation (lines) and trapping (half parabola) domains.

each wave amplitude, the output beam VDF is recorded after interaction of the test beam with the wave propagating along the helix: the VDF is obtained by scanning the retarding voltage with a step of 61 mV. The zero level of each VDF is defined as the mean trochoidal collector current averaged over 50 velocities in the tail of the VDF where only noise is recorded. Each beam VDF is then normalized to keep the beam current constant. Figure 2(a) is obtained after linear interpolation by a MATLAB treatment of the recorded output VDFs, giving a 3D plot of the VDF in the (ϕ_0, v) plane, where ϕ_0 is the wave amplitude measured at the launching antenna position. An estimate of the helix wave amplitude ϕ_0 is obtained by determining the emitting probe coupling coefficient using three probes measurements [10].

When the wave amplitude is null, Fig. 2(a) shows that the VDF exhibits a single peak centered at $v_b = 3.82 \times 10^6 \text{ m/s}$, which is the entrance velocity of the test beam with current $I_b = 175 \text{ nA}$. Thus, in the absence of the wave, the test beam propagates unperturbed along the helix. When the wave amplitude is gradually increased, this single peak gives birth to two peaks whose separation increases. This is explained easily. Let the wave potential be $\phi(z) \sin(k_{0r}z - 2\pi ft)$. The wave propagates with phase velocity $v_\phi = 2\pi f/k_{0r} = 4.06 \times 10^6 \text{ m/s}$ given by the dispersion relation of the helix at 30 MHz. As $v_b > v_\phi + 2\sqrt{\eta\phi_0}$, the beam electrons are outside the trapping velocity region of the wave and are nonresonant with the wave; $\eta = |q|/m$ is the electron charge to mass ratio. Neglecting the wave spatial damping, their motion mainly consists of a velocity modulation with amplitude $\eta\phi_0/|v_\phi - v_b|$ around their initial velocity v_b . This estimate is obtained by first order perturbation theory with respect to the constant helix wave amplitude ϕ_0 around the electron unperturbed free motion with constant velocity v_b . Averaging over the arbitrary initial phase of the electron in the wave yields two peaks at the maximum and minimum electron velocity for the VDF, as usual for a sinusoidal motion.

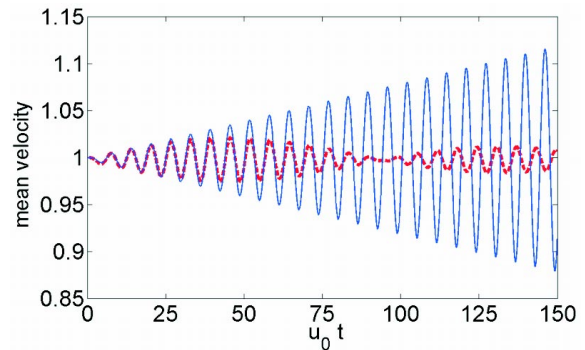


FIG. 3 (color online). Exact value (dashed curve) and second order estimate (continuous curve) of the velocity averaged over initial position vs time, for $\epsilon = 0.04$, $u_0 = 1$.

Figure 2(b) gives a 2D contour plot of the VDF in the (ϕ_0, v) plane, with the two continuous lines corresponding to a linear symmetric fit as predicted by the above modulation estimate. We observe a systematic deviation from this simple estimate toward v_ϕ as the wave amplitude increases. For v_b larger than v_ϕ we have also observed a deviation toward v_ϕ . This deviation is witness to a synchronization of the electrons with the wave.

It is explained by considering the motion of individual test electrons. Let $x = k_0 r z - 2\pi f t$, $u = k_0 r v - 2\pi f$, and $\epsilon = \eta k_0 r^2 \phi_0$. Then the motion of a test electron with initial position x_0 and velocity u_0 is described by the differential equation $\ddot{x} = \epsilon \cos(x)$, where the dots denote derivation with respect to time t . This equation of the classical nonlinear pendulum is analytically integrable using Jacobi elliptic functions for each particle. Averaging over the initial position uniformly distributed over one wavelength, we get the dashed curve of Fig. 3 for a particle with initial velocity u_0 outside the trapping velocity domain of the wave (the libration velocity domain of the pendulum). Using perturbation theory of second order in ϵ around the unperturbed motion $x = x_0 + u_0 t$, we estimate this deviation and obtain

$$\langle u \rangle = u_0 + \epsilon^2 \left\{ \frac{[\cos(u_0 t) - 1]}{u_0^3} + t \frac{\sin(u_0 t)}{2u_0^2} \right\} + \dots \quad (1)$$

for the beam velocity averaged over x_0 . This estimate is shown as the continuous curve in Fig. 3. As expected, this estimate with its secular term diverges from the exact prediction after a finite time T . This time can be estimated as the inverse of the width of the frequency spectrum associated to the exact velocity modulation (estimated by ϵ/u_0 to first order in ϵ for a particle with initial velocity u_0); i.e., $T = u_0/\epsilon$. The continuous curve shows that the average velocity of the particles having a given initial velocity but arbitrary phase oscillates with the pulsation

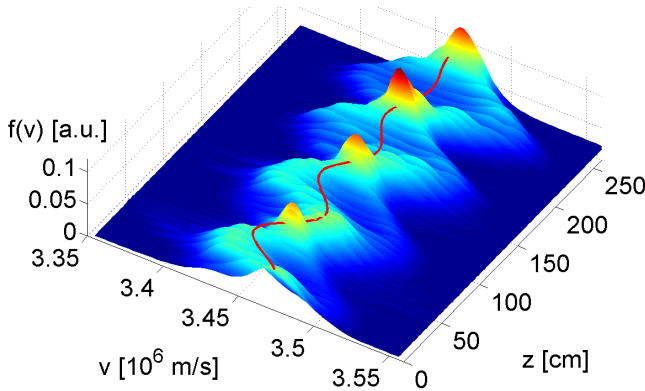


FIG. 4 (color online). Measured velocity distribution function for a single wave with phase velocity 4.06×10^6 m/s and amplitude 18 mV vs emitting antenna position z from the gun end; second order estimate of mean test beam velocity (continuous curve).

u_0 which corresponds to the velocity mismatch between the wave and the beam. At the output of the TWT, we observe the test beam after interaction over a given length L with the wave. This produces the overall synchronization of Fig. 2(b) because $t = L/v_b = 0.13 \mu\text{s}$ is smaller than $2\pi/u_0 = v_\phi/(f|v_b - v_\phi|) = 0.54 \mu\text{s}$, so that the beam experiences the first nonlinear synchronization of Fig. 3 (which occurs at the first minimum of either curve, i.e., for $u_0 t \sim 4$).

We now keep the wave amplitude constant and vary the interaction length z by moving the emitting antenna along the helix. Figure 4 is obtained by superposing the test beam VDF measured at the output of the helix for 100 different antenna positions starting at the gun end of the TWT and spaced every 2.5 cm. We first notice a periodic velocity bunching of the VDF with a spatial period L_b which can be derived as follows. Intuitively, if the electron transit time L_b/v_b over a length L_b differs from the wave propagation time L_b/v_ϕ by one wave period $1/f$, all electrons have undergone a complete acceleration-deceleration cycle and thus recover their initial velocity. This yields $L_b = v_b v_\phi / (f|v_b - v_\phi|) = 0.76$ m which is indeed the measured periodic bunching length. The bunching explains why the VDF is peaked in Fig. 4; indeed there is a minimum spreading of the VDF. Finally note that the amplitude of the beam velocity modulation increases with z because, when the probe comes closer to the output, the wave amplitude is less damped along the SWS.

A closer look at the color contours of Fig. 4 shows that the average velocity of the test beam oscillates with z . The continuous curve superimposed in the contour plot is the second order estimate of the phase averaged velocity for the measured wave amplitude of 0.10 V when the wave damping $k_{0i} = 0.13 \text{ m}^{-1}$ is also included [Eq. (1) corresponds to $k_{0i} = 0$]. The same curve is plotted in Fig. 5 and compared to the mean beam velocity computed from the measured VDFs of Fig. 4. As shown by the typical error bar of Fig. 4, the agreement between measurement and theory is very good.

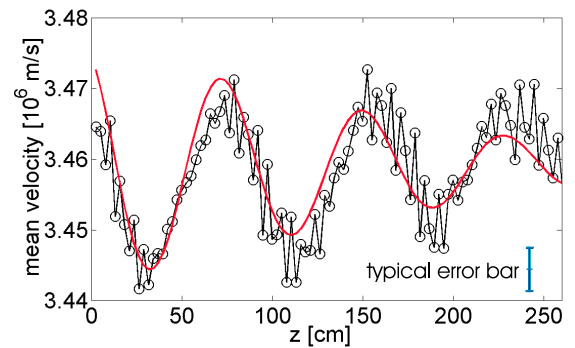


FIG. 5 (color online). Mean test beam velocity measured from Fig. 4 (shaggy curve joining data), estimated by second order perturbation theory (smooth curve).

We now recall why the kind of synchronization displayed by Fig. 2(b) is at the origin of Landau damping. We first explain this synchronization intuitively [5]. Consider two passing particles with the same velocity v located at $t = 0$ symmetrically with respect to the wave potential bottom. At first order in perturbation theory, they have exactly opposite accelerations over a small time δt . However, second order perturbation theory incorporates the fact that the particle whose velocity is going away from the phase velocity experiences later on a smaller acceleration than the one coming closer. Therefore the second order average effect is indeed a synchronization over a small time $\delta t \lesssim 4/u_0$. These particles may be cast in two groups: one slower than the wave, and one faster. If the particle VDF has a negative slope at the wave phase velocity, particles gain overall momentum in the synchronization process, and vice versa for a positive slope. The collective effect of momentum balance is a feedback on the wave which loses or gains momentum, i.e., damps or grows accordingly. This is the mechanical origin of Landau damping for a single wave.

We can also estimate more precisely the range of velocities where wave-particle momentum exchange is maximum. From the argument of the cosine in Eq. (1), we see that δt must be compared with $\tau(u_0) = |u_0|^{-1}$ typically. Now imagine the wave amplitude evolving exponentially in time with a growth or damping rate γ . Then, after a time $|\gamma|^{-1}$, the particles are no longer subjected to the same “constant” amplitude wave. This sets a time bound on the applicability of the perturbative picture of Eq. (1). Strongly nonresonant particles, such that $\tau(u_0) \ll |\gamma|^{-1}$, have the vanishing nonlinear velocity change displayed for large t by the dashed curve in Fig. 3. Resonant or almost resonant particles, such that $\tau(u_0) \gg |\gamma|^{-1}$, have the vanishing nonlinear velocity change displayed by the curves in Fig. 3 for $t \approx 0$. In contrast, particles such that $\tau(u_0) \sim |\gamma|^{-1}$, i.e., $|u_0| \sim \gamma$, have the kind of synchronization displayed in Fig. 2(b).

This intuitive picture can be made rigorous by describing wave-particle interaction as the self-consistent evolution of a one-dimensional system of N particles in one electrostatic wave [7]. It is defined by a Hamiltonian [3,11] which describes on an equal footing the evolution of the wave, with conjugate variables (I, θ) , and that of the particles, with conjugate variables (p_l, z_l) ; I is the wave energy divided by $2\pi f$. The corresponding dynamics conserve the total wave-particle momentum $P = \sum_{l=1}^N p_l + k_0 I$. This constant reveals that a change of particle momentum impacts on the wave amplitude $\phi \propto I^{1/2}$. Reciprocally, the overall particle momentum change is quadratic in the wave amplitude as hinted by Eq. (1). The self-consistent Hamiltonian enables us to recover the Landau effect for the wave and to prove that it corresponds to a synchronization of the particles with the wave [3–5]; the time average force corresponding to this synchroniza-

tion is maximum for particles with a relative velocity $|v| \sim |\gamma|/(\sqrt{3}k_0)$ in the wave frame.

In conclusion, a basic wave-particle interaction experiment has been performed in a TWT with a test electron beam. The observed amplitude and spatial evolution can be directly related to the temporal evolution usually investigated in perturbation theory. It shows the first direct experimental evidence of beam synchronization effects responsible for Landau damping of a single wave. For a broad spectrum of waves, this damping is theoretically linked to a quasilinear diffusion [3–5,12,13], and the recent experimental proof of the transition to chaos in the presence of two or more waves [14] was a step in the direction of experimental evidence for such a diffusion.

The authors are grateful to Y. Elskens for fruitful discussions and a critical reading of the manuscript and to J.-C. Chezeaux, D. Guyomarc’h, P. Martinez, and B. Squizzato for technical assistance. A. Macor benefits from a grant by Ministère de la Recherche.

*Electronic address: doveil@up.univ-mrs.fr

†Electronic address: escande@up.univ-mrs.fr

‡Electronic address: macor@up.univ-mrs.fr

- [1] L. Landau, J. Phys. (USSR) **10**, 25 (1946); J. H. Malmberg and C. B. Wharton, Phys. Rev. Lett. **17**, 175 (1966).
- [2] A. Fasoli *et al.*, Phys. Rev. Lett. **63**, 2052 (1989); M. Sarfaty, S. De Souza-Machado, and F. Skiff, Phys. Rev. Lett. **80**, 3252 (1998).
- [3] Y. Elskens and D. F. Escande, *Microscopic Dynamics of Plasmas and Chaos*, (IoP Publishing, Bristol, 2003).
- [4] D. F. Escande, S. Zekri, and Y. Elskens, Phys. Plasmas **3**, 3534 (1996).
- [5] D. F. Escande and Y. Elskens, Plasma Phys. Controlled Fusion **45**, A115 (2003).
- [6] G. Dimonte and J. H. Malmberg, Phys. Fluids **21**, 1188 (1978).
- [7] I. N. Onischenko *et al.*, JETP Lett. **12**, 281 (1970); T. M. O’Neil, J. H. Winfrey, and J. H. Malmberg, Phys. Fluids **14**, 1204 (1971).
- [8] K. W. Gentle and C. W. Roberson, Phys. Fluids **14**, 2780 (1971); K. W. Gentle and J. Lohr, Phys. Fluids **16**, 1464 (1973).
- [9] D. Guyomarc’h and F. Doveil, Rev. Sci. Instrum. **71**, 4087 (2000).
- [10] J. H. Malmberg, T. H. Jensen, and T. M. O’Neil, in *Plasma Physics and Controlled Nuclear Fusion Research* (IAEA, Vienna, 1966), Vol. I, p. 683.
- [11] H. E. Mynick and A. N. Kaufman, Phys. Fluids **21**, 653 (1978); M. Antoni, Y. Elskens, and D. F. Escande, Phys. Plasmas **5**, 841 (1998).
- [12] D. F. Escande and Y. Elskens, Phys. Plasmas **10**, 1588 (2003).
- [13] A. A. Vedenov, E. P. Velikhov, and R. Z. Sagdeev, Nuclear Fusion Suppl. **2**, 465 (1962); W. E. Drummond and D. Pines, Nuclear Fusion Suppl. **3**, 1049 (1962).
- [14] F. Doveil, Kh. Auhmani, A. Macor, and D. Guyomarc’h, Phys. Plasmas **12**, 010702(L) (2005).